Photometry: Mare vs Highlands. A. K. Boyd and M. S. Robinson, School of Earth and Space Exploration, Arizona State University, Tempe, AZ, USA (aboyd@ser.asu.edu)

Introduction: Lighting conditions beneath the Lunar Reconnaissance Orbiter (LRO) systematically vary from month-to-month providing the opportunity to characterize photometric properties across the full range of surface materials. Off nadir campaigns and multi-temporal imaging increase the range of photometric angles observed. As a result, the Lunar Reconnaissance Orbiter Camera (LROC) Narrow Angle Camera (NAC) has acquired a robust set of broadband globally distributed photometric observations (450 – 700 nm).

Each NAC has a 2.85° field-of-view [**1**], thus the photometric angles of incidence (angle of sub-solar vector relative to the surface normal) and emission (angle of camera boresight vector relative to the surface normal) [**2**] vary dominantly from topography in a single image, with phase angle (angle between emission and incidence vectors) changing very little across an image. We derived five global empirical photometric solutions from a set of NAC images to enable quantitative comparisons of reflectance values across the Moon. The globe was divided into four compositional and maturity units (±90° latitude) using optical maturity (OMAT) values [**3**] and a mare boundary shapefile [**4**]. To compute the Mean Moon Photometric Functions (MMPFs) including Mature Highlands (MH), Immature Highlands (IH), Mature Mare (MM), and Immature Mare (IM), data from 5 million off nadir LROC NAC image tiles (1 km x 1 km) were reduced, similar to the method described in Boyd et al. [**5**], but with more off nadir NAC images including an extended latitude range (±90°) [**5**].

Method: NAC images were selected based on incidence angle (<91°), emission angle (85°> e >2°), and beta angle (orbital plane and solar vector separation; 30°>β>-30°). Only images with data quality IDs < 16 were included in the study.

Data Preparation: Radiometrically calibrated I/F [**6,7**] were binned to 1 km x 1 km pixel scales enabling accurate photometric angle calculations from the GLD100 [**8**], while maintaining a manageable dataset size. Photometric angles (local phase (g), local emission (e), and local incidence (i) angles), latitude, and longitude were calculated for each tile. Only tiles with phase angles >10°, incidence angles <65°, and emission angles <85° were used in fitting.

The I/F values and photometric angles were reduced with a linear least squares fit for each MMPF. The response variable log(I/F) and dependent variables g, cos(e), and cos(i) were calculated and stored for use in curve fitting.

Curve Fitting: The I/F values were binned by photometric angles and only the average for each bin was used

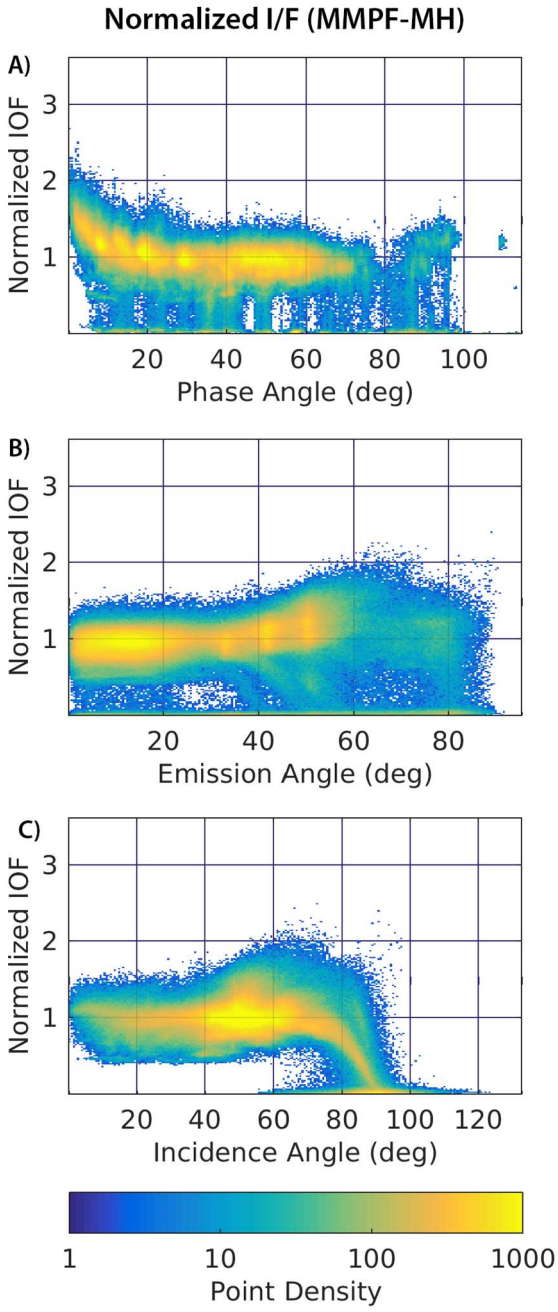

Figure 1: *The MMPF-MH is valid for phase angles >10° (I/F increases dramatically <10° phase angle) [A], all emission angles [B], and incidence angles <65° (I/F decreases rapidly >65° incidence angle) [C]. In the valid range, the normalized I/F (I/F/model) shows little trending. Outside of the valid geometry range, the MMPF-MH is smooth, but increases in error magnitude as the distance from the valid range increases.*

for fitting. This removes bias in the MMPFs of higher point density regions (near nadir and larger incidence angles).

After the preliminary fitting, the normalized I/F was computed for all original data points, and outliers were identified as points greater than three standard deviations from the mean normalized I/F. With outliers excluded (<5%,>95%), the mean for each bin was recomputed, and the MMPFs were fitted using the bins.

$$\log\left(\frac{I}{F}\right) = k0 + k1\,g + k2\cos(e) + k3\cos(i)$$

Mean Moon Photometric Function (MMPF), log(IOF) depends linearly on phase (g), emission (e), and incidence (i) angles.

	k0	k1	k2	k3
OMAT>0.35	-2.939	-0.013	0.051	1.815
MMPF-IH	-2.588	-0.013	-0.240	1.260
MMPF-MH	-2.649	-0.013	-0.274	0.965
MMPF-IM	-2.547	-0.013	-0.433	0.645
MMPF-MM	-2.572	-0.013	-0.351	0.328

Table 1: *Coefficients for the Mean Moon Photometric Functions.*

Results and Discussion: The MMPFs are designed as a general purpose correction for lunar terrains. The functions are well fit for phase angles between 10° and 100°, all emission angles, and incidence angles <65° corresponding to roughly 60% of all NAC images within 65° latitude of the equator. The solutions presented here improved upon that of Boyd et al. [**5,9**] in terms of pixel scale and fit accuracy due to significantly more off nadir observations and using lunar terrain classifications.

If using only one MMPF, the mature highlands (MMPF-MH) should be used. The MMPF-MH will work for the largest percentage of the lunar surface; however, if working with locations where the terrain type is known, the MMPF for that terrain could see up to a 6% improvement in the accuracy of normalized I/F (Fig 2).

The models show that reflectance is positively corelated with OMAT values with the most immature highlands having the highest model values. However, the mature highlands classification has higher modeled reflectance than both mare classifications indicating that composition has a greater effect on reflectance than maturity for the Moon (Fig 2A).

When comparing the shapes of the model curves, the immature mare model (MMPF-IM) is found to be the strongest backscattering of the terrains investigated, followed by the most immature highlands (0.35<OMAT), and immature highlands (MMPF-IH). Mature highlands and mature mare terrains have a surprisingly similar shape, suggesting that maturity has a greater effect on photometric response than composition for lunar soils (Fig 2B).

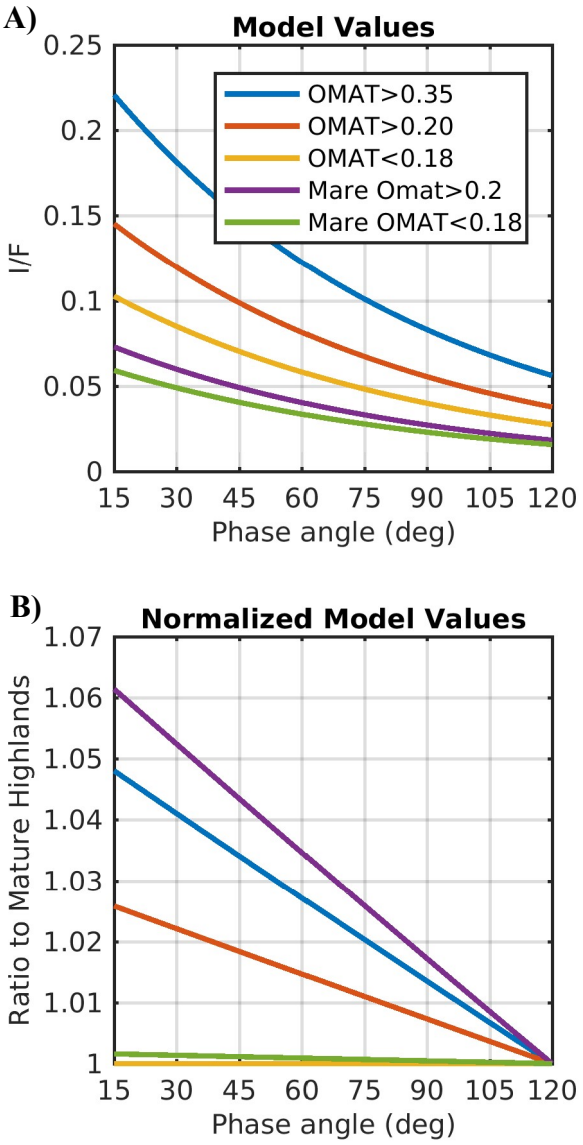

Figure 2: *MMPF values [A] and normalized model values [B] against phase angle for i=30° and e=0°. The higher negative slopes indicate surfaces that are more backscattering. The model for immature mare has the highest amount of backscatter followed by extremely fresh non-mare terrains.*

References: [1] Robinson et al. (2010) *Space Science Rev.* 150: 81-124. [2] Hapke B. (2012) Cambridge University Press. [3] Lucey et al. (2000) *JGR* 105. [4] Nelson et al. (2014). *LPSC* 45 #2861. [5] Boyd et al. (2017) *3rd Planetary Data Workshop* #1986. [6] Becker, K.J., et al. (2013) *LPSC* 44 #2829 [7] Humm, D. C. et al. (2016) *Space Sci. Rev.* 200. [8] Scholten, F. et al. (2012). *JGR*, 117. [9] Boyd et al. (2014) LPSC 45 #2826